

# The contribution of spike threshold to the dichotomy of cortical simple and complex cells

Nicholas J Priebe<sup>1</sup>, Ferenc Mechler<sup>2</sup>, Matteo Carandini<sup>3</sup> & David Ferster<sup>1</sup>

The existence of two classes of cells, simple and complex, discovered by Hubel and Wiesel in 1962, is one of the fundamental features of cat primary visual cortex. A quantitative measure used to distinguish simple and complex cells is the ratio between modulated and unmodulated components of spike responses to drifting gratings, an index that forms a bimodal distribution. We have found that the modulation ratio, when derived from the subthreshold membrane potential instead of from spike rate, is unimodally distributed, but highly skewed. The distribution of the modulation ratio as derived from spike rate can, in turn, be predicted quantitatively by the nonlinear properties of spike threshold applied to the skewed distribution of the subthreshold modulation ratio. Threshold also increases the spatial segregation of ON and OFF regions of the receptive field, a defining attribute of simple cells. The distinction between simple and complex cells is therefore enhanced by threshold, much like the selectivity for stimulus features such as orientation and direction. In this case, however, a continuous distribution in the spatial organization of synaptic inputs is transformed into two distinct classes of cells.

Hubel and Wiesel first defined simple and complex cells of the primary visual cortex according to whether their receptive fields could be subdivided into separate ON and OFF subregions<sup>1,2</sup>. This classification scheme is still widely used and correlates well with a cell's laminar position and synaptic connectivity<sup>3–5</sup>. A more quantitative method of distinguishing the two cell classes relies on responses to drifting gratings<sup>6</sup>. The firing rates of simple cells are strongly modulated at the grating temporal frequency and therefore have a large fundamental Fourier component ( $R_1$ ) relative to the mean elevation in firing ( $R_0$ ); conversely, complex cells respond with an elevation in firing rate that is only weakly modulated, so they have a small  $R_1$  relative to  $R_0$ . The modulation ratio  $R_1/R_0$ , in a large population of cortical cells, forms a clearly bimodal distribution, the two groups corresponding well with Hubel and Wiesel's definition of simple and complex<sup>6</sup>. The ratio is therefore widely used to distinguish simple and complex cells, and its bimodal distribution provides strong evidence that the two classes are fundamentally distinct and receive distinct patterns of synaptic inputs<sup>7</sup>.

The rationale for using the  $R_1/R_0$  measure to identify simple and complex cells is intimately related to Hubel and Wiesel's hierarchical model of processing in visual cortex. In the model, simple cells receive input from ON- and OFF-center geniculate relay cells with nonoverlapping receptive field centers<sup>1,2,8</sup>. The synaptic input from these relay cells is synchronously modulated as the alternating light and dark bars of a drifting grating enter and leave the distinct ON and OFF subregions of each relay cell's receptive field. This modulation in excitatory synaptic input gives rise to a large modulation in the membrane potential ( $V_1$ ) relative to the increase in the mean potential ( $V_0$ ). The resulting high value of the membrane potential

modulation index,  $V_1/V_0$ , leads to a strongly modulated firing rate (high  $R_1/R_0$ ). Complex cells, in turn, are thought to receive input from many simple cells with overlapping, but slightly offset, receptive fields<sup>9–12</sup>. Because a drifting grating encounters the subregions of the different component simple cells asynchronously, these inputs should generate a relatively steady, unmodulated elevation in membrane potential (low  $V_1/V_0$ ) and therefore a steady, unmodulated elevation in firing rate (low  $R_1/R_0$ ). By this reasoning, the bimodality of the  $R_1/R_0$  distribution in the cortical population argues strongly for the existence of two clearly distinct patterns of synaptic input, and by extension a fundamental distinction between the synaptic circuitry of simple and complex cells.

Mechler and Ringach have proposed an alternative to the synaptic connectivity model of bimodality in the modulation index<sup>13</sup>. In their model, the distribution of the modulation ratio of the membrane potential responses ( $V_1/V_0$ ) is unimodal. There are still cells at one end of the distribution that receive the pure, simple-like connections described by the hierarchical model, and cells at the other end that receive pure, complex-like connections. But Mechler and Ringach propose that there are many cells in the middle of the distribution that receive a mix of inputs and have intermediate values of  $V_1/V_0$ . The bimodal distribution in  $R_1/R_0$  then emerges as a result of the highly nonlinear relationship between membrane potential and firing rate that is inherent in the spike threshold. If this model were correct, it would not be necessary to postulate a fundamental dichotomy between the circuitry that shapes simple and complex cell responses. Cortical connections would instead form a continuum.

To determine whether the spike threshold enhances the difference between simple and complex cells, we have compared  $R_1/R_0$  and

<sup>1</sup>Department of Neurobiology and Physiology, Northwestern University, 2205 Tech Drive, Evanston, Illinois 60208, USA. <sup>2</sup>Department of Neurology and Neuroscience, Medical College of Cornell University, New York, New York 10021, USA. <sup>3</sup>Smith-Kettlewell Eye Research Institute, 2318 Fillmore Street, San Francisco, California 94115, USA. Correspondence should be addressed to D.F. (ferster@northwestern.edu).

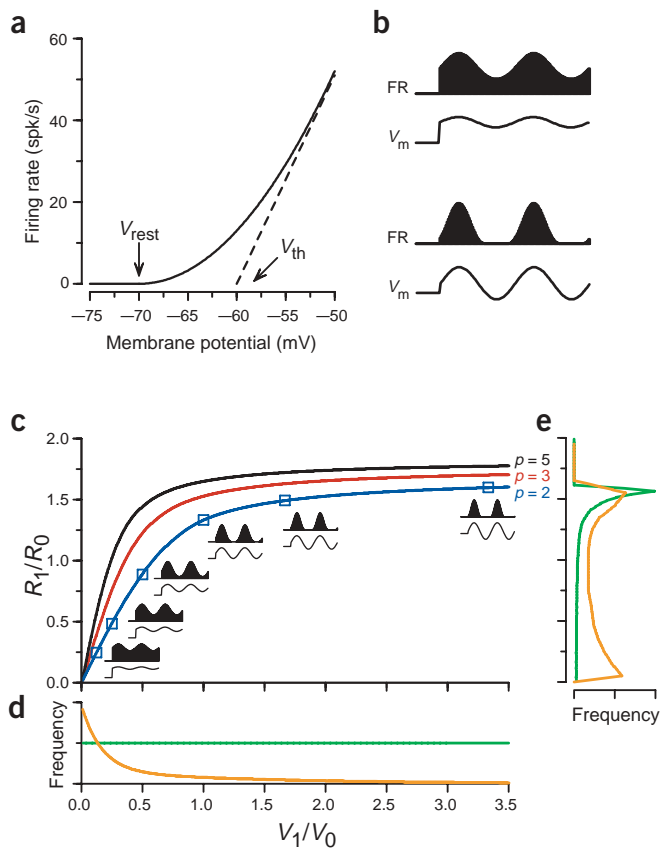


**Figure 1** The nonlinear transformation from the voltage modulation ratio to the firing rate modulation ratio. **(a)** The transformation between voltage and spiking response for two models: the solid line indicates the transformation for the power-law model and the dashed line indicates the transformation for the threshold-linear model (see Methods for details). **(b)** Transformations of membrane potential ( $V_m$ , traces) to firing rate (FR, filled bars) for two model voltage modulation ratios. Both panels show the membrane potential to firing rate transformation assuming the power-law model with an exponent  $p = 2$ . Top panel,  $V_1/V_0 = 0.24$  and  $R_1/R_0 = 0.47$ ; bottom panel,  $V_1/V_0 = 1.67$  and  $R_1/R_0 = 1.5$ . **(c)** The nonlinear transformation of the voltage modulation ratio (abscissa) to the firing rate modulation ratio (ordinate) for power-law models with a threshold at  $V_{rest}$  and various exponents, including  $p = 2$  (blue curve),  $p = 3$  (red curve) and  $p = 5$  (black curve). The curves are derived in the **Supplementary Note** online, following Mechler and Ringach<sup>13</sup>. Connected by the blue curve, each square shows the mapping of a particular voltage modulation ratio in model neurons that use the power law with exponent  $p = 2$ . Insets indicate the corresponding transformation of membrane potential (traces) to firing rate (filled bars). **(d)** An even distribution (green trace) and highly skewed distribution (orange trace) of the voltage modulation ratio. **(e)** The firing rate modulation distributions resulting from the even distribution (green trace) and skewed distribution (orange) found in **(d)** when transformed by the relationship dictated by the power law with exponent  $p = 2$  (blue curve in **(c)**).

$V_1/V_0$  in intracellular recordings from neurons in the cat primary visual cortex. We found that the distribution of  $V_1/V_0$  is indeed unimodal, though highly skewed. And as predicted by Mechler and Ringach, the concurrent bimodal distribution of  $R_1/R_0$  can be explained quantitatively by the nonlinear effects of spike threshold. In addition, we quantified the distinction between simple and complex cells on the basis of the segregation of the ON and OFF responses within the receptive field, which we mapped by flashing bright and dark spots. As for grating responses, cortical cells formed two distinct populations when subfield segregation was based on spiking responses, whereas they formed a single, continuous distribution when segregation was based on membrane potential responses. Thus, our data suggest that the dichotomy between simple and complex cells arises from a specific unimodal distribution of synaptic inputs transformed by the mechanism for spike generation.

## RESULTS

The key proposal made by Mechler and Ringach to account for the observed bimodal distribution of  $R_1/R_0$  lies in the nonlinear transformation between membrane potential and firing rate<sup>13</sup>. The expansive nonlinear relationship between voltage and spiking (Fig. 1a) tends to enhance the modulated component of the intracellular response for most cells, as shown in two model neurons in Figure 1b. Here, we have modeled the membrane response of each neuron as the sum of a steady elevation ( $V_0$ ) and a sinusoidal modulation ( $V_1$ ); this response is transformed to firing rate by a power law (Fig. 1a) in which firing rate is proportional to the voltage above rest raised to the power of 2 ( $p = 2$ )<sup>14,15</sup>.

In the top example of Figure 1b,  $V_1/V_0$  is at the low value of 0.24. The squaring operation of the voltage-to-spiking transformation,

however, selectively enhances the modulation; the difference between the peak and the trough of the response is amplified by the squaring more than the mean level is amplified, so that  $R_1/R_0 = 0.47$ , which is about twice the value of  $V_1/V_0$ . The second model neuron in Figure 1b has a higher voltage modulation ratio,  $V_1/V_0 = 1.67$ . For this cell, the power law slightly reduces the large difference between peak and trough ( $R_1/R_0 = 1.5$ ) because the large membrane potential modulation carries the membrane potential significantly below rest, whereas the firing rate has a lower bound of 0. The complete relationship between  $V_1/V_0$  and  $R_1/R_0$  for the power-law nonlinearity with an exponent  $p = 2$  is shown in Figure 1c (blue curve). In general, the nonlinearity of the relationship amplifies low values ( $V_1/V_0 < 1.46$ ) by a factor of up to 2, whereas it attenuates high values in the saturating portion of the curve ( $V_1/V_0 > 1.46$ ). That is, for the sharply rising portions ( $V_1/V_0 < 0.68$ ) of the curve in Figure 1c, the relationship between  $R_1/R_0$  and  $V_1/V_0$  is expansive: a narrow range of  $V_1/V_0$  is spread out into a wide range of  $R_1/R_0$ . For the shallow portions of the curve, just the opposite is true: a wide range of  $V_1/V_0$  is compressed into a narrow range of  $R_1/R_0$ . Note that the point at which the relationship between  $R_1/R_0$  and  $V_1/V_0$  changes from an expansive to a compressive nonlinearity depends on the exponent,  $p$ , which defines the power-law relationship between voltage and spiking. The higher  $p$  is, the lower the dividing point (Fig. 1c, red and black curves). In addition, the higher  $p$  is, the higher the saturating value of  $R_1/R_0$ .

By itself, the relationship shown in Figure 1c does not transform an even distribution of  $V_1/V_0$  (Fig. 1d, green curve) into a bimodal distribution of  $R_1/R_0$ , but instead gives rise merely to a single skewed peak (Fig. 1e, green curve). It appears, therefore, that the  $V_1/V_0$ -to- $R_1/R_0$  transformation, even though it can dramatically transform the  $V_1/V_0$  distribution, by itself cannot completely explain the bimodality of  $R_1/R_0$ . A bimodal distribution of  $R_1/R_0$  can emerge (Fig. 1e, orange curve), however, when there is a highly skewed distribution of  $V_1/V_0$  that is appropriately matched in shape to the nonlinearity in the  $V_1/V_0$ -to- $R_1/R_0$  transformation. In the orange curve of Figure 1d, for example, the long tail in the  $V_1/V_0$  distribution that roughly matches the saturating regions of the curves in Figure 1c gets compressed by the nonlinear transformation into a second peak in the  $R_1/R_0$  distribution, giving rise to the bimodal distribution in the orange curve of Fig. 1e. For Mechler and

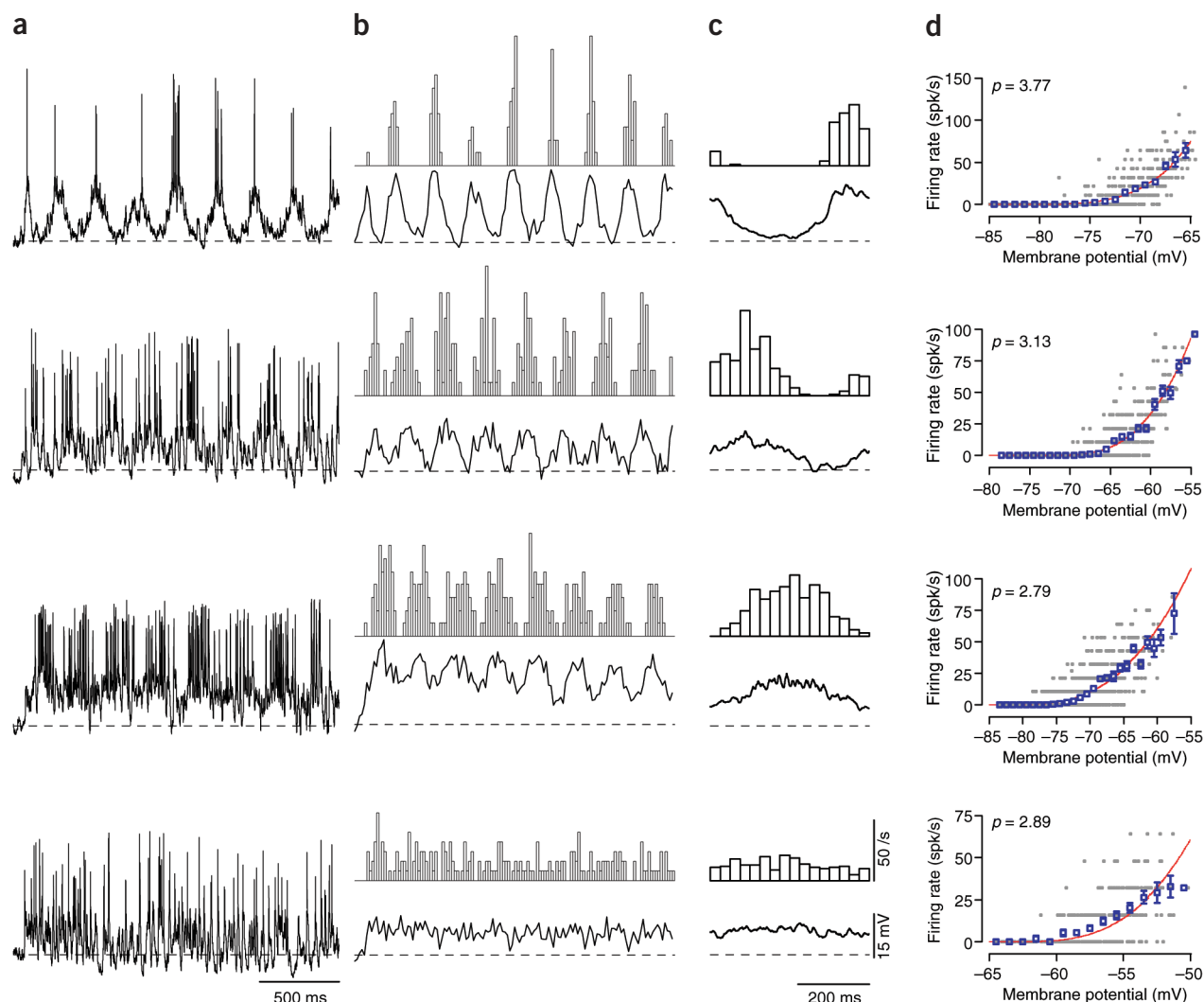


**Figure 2** Intracellular responses to drifting gratings in four example neurons. Gratings had optimal orientation, spatial frequency and direction. (a) Responses of four neurons to a grating moving at 2 Hz and 64% contrast. The traces include 4 s of stimulation after 0.25 s of blank stimulus (0.1 s shown). The dashed line indicates each neuron's resting membrane potential ( $V_{rest}$ ). (b) Trial-averaged firing rate histograms (upper panel) and voltage traces. (c) Cycle-averaged firing rate histograms and voltage traces. Spikes were removed from voltage traces prior to averaging by using a 4-ms median filter<sup>39</sup>. The spike responses of these cells (from top to bottom, in spikes/s) were as follows:  $R_0$ : 11.17, 21.00, 24.17, 13.06;  $R_1$ : 19.82, 24.51, 21.54, 3.68; the intracellular responses were (in mV)  $V_0$ : 5.49, 9.73, 13.77, 6.31;  $V_1$ : 8.25, 4.40, 4.69, 1.05. (d) Transformation between average voltage and firing rate. The blue symbols indicate the average firing rate when membrane potential is binned in 1-mV steps (error bars are s.e.m.). The red curve indicates the power-law function that best fit the data (see Methods).

Ringach's proposal to hold, then, two conditions should be met: (i) a nonlinear transformation between voltage and spiking and (ii) an appropriate shape of the  $V_1/V_0$  distribution.

### Distinguishing simple and complex cells with gratings

To test these two predictions, we recorded intracellularly from 102 neurons in area 17 of the cat and compared the modulation ratios derived from spike rate and membrane potential. Sample membrane potential traces recorded in response to drifting gratings at the preferred orientation and spatial frequency are shown for four cells in Figure 2a, along with trial-by-trial and cycle-by-cycle averages of the membrane potential and firing rate (Fig. 2b,c). The illustrated cells span the range of observed  $R_1/R_0$  ratios: the top cell lies in the simple cell range, with large modulations of membrane potential and firing rate, whereas the bottom cell shows the very weakly modulated

responses typical of complex cells. Figure 2d contains a scatter plot of the relationship between mean membrane potential and mean firing rate for each 30-ms epoch of the grating responses (gray points). The blue open symbols show mean and standard deviation of the firing rate for each 1-mV bin in the graph. The gray points are fit to a power law (red curves, see Methods), the exponent of which is shown in the upper left of each graph.

Histograms of  $R_1/R_0$  and  $V_1/V_0$  are shown in Figure 3a and b for the population of 102 cortical neurons stimulated with gratings of the preferred orientation and spatial frequency. As shown previously, the  $R_1/R_0$  distribution was strongly bimodal<sup>6</sup>. In contrast, the  $V_1/V_0$  distribution was not at all bimodal, although it was heavily skewed toward values less than 1. While the mean  $V_1/V_0$  was very different for simple and complex cells (as defined from  $R_1/R_0$ ), there was considerable overlap in the distributions, such that simple and complex cells

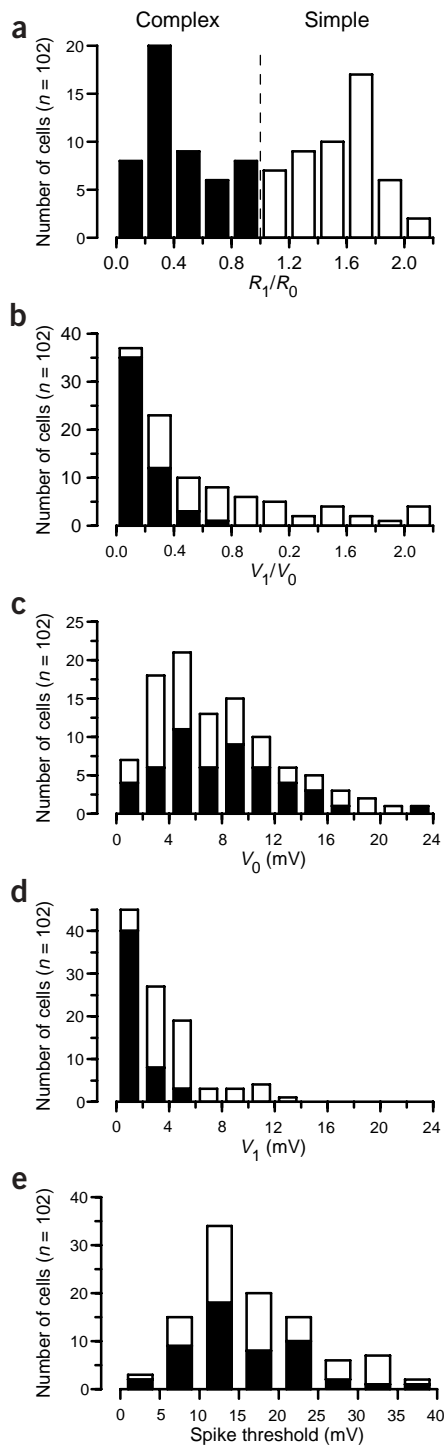


**Figure 3** The distribution of responses to drifting gratings across our sample population. Dark bars indicate neurons classified as complex ( $R_1/R_0 < 1$ ) and open bars indicate neurons classified as simple ( $R_1/R_0 > 1$ ). (a) The distribution of  $R_1/R_0$  was significantly bimodal (Hartigan's dip test,  $P < 0.02$ ). Firing rate modulation values greater than 2.2 were included in the highest bin. (b–e) The distributions of  $V_1/V_0$  (b),  $V_1$  (c),  $V_0$  (d) or spike threshold (measured relative to the resting potential; e) were not bimodal (Hartigan's dip test,  $P > 0.5$ ).

Cells with higher thresholds, for example, will have higher effective values of the power-law exponent  $p$  (see below), which would in turn alter the amplification or attenuation of  $R_1/R_0$  at different values of  $V_1/V_0$ . The overall distribution of spike threshold was unimodal (Hartigan's dip test<sup>16</sup>,  $P = 0.6$ ), however, and distribution of thresholds for simple cells overlapped almost completely with that of complex cells (Fig. 3e). The 3.5-mV difference between mean thresholds for simple and complex cells was small compared to the 39-mV range of values (mean simple threshold =  $19.8 \pm 1.32$  mV; mean complex threshold =  $16.3 \pm 1.1$  mV). Therefore, none of the intracellular properties of the cells examined here—spike threshold,  $V_0$  or  $V_1$  taken individually, the  $V_1/V_0$  ratio or the correlation between  $V_0$  and  $V_1$ —showed a strong bimodality by which simple and complex cells could be unequivocally defined.

The relationship between  $V_1/V_0$  and  $R_1/R_0$  for the sample population is shown in Figure 4a, together with the histograms of each of the two variables (Fig. 4b and c). The relationship is reminiscent of the theoretical relationships shown in Figure 1c (smooth curves in Fig. 4a): as  $V_1/V_0$  increases,  $R_1/R_0$  tends to saturate. There is considerable scatter in the relationship. This scatter is not unexpected given that different neurons have different values of  $p$  in the power-law relationship between membrane potential and spike rate, and  $p$  in turn affects the exact relationship between  $V_1/V_0$  and  $R_1/R_0$ , as reflected in the theoretical curves. If variation in  $p$  is responsible for the scatter in Figure 4a, then the points representing cells with similar values of  $p$  should cluster close to the curve of the corresponding  $p$  value. To facilitate a qualitative evaluation, we color-coded the symbol for each cell according to the exponent of its input-output curve; cells with  $p$  near 2 were colored black, cells with  $p$  near 3 were colored red, and cells with  $p$  near 5 were colored blue. We observed a clear tendency for the individual points to cluster near the corresponding theoretical curve.

To quantify how well the model can predict  $R_1/R_0$ , we plotted the measured  $R_1/R_0$  against the  $R_1/R_0$  that was predicted from  $V_1/V_0$  and the fitted  $p$  (Fig. 4d). The predicted values were highly correlated with the measured values ( $R^2 = 0.72$ ). The slope of the correlation (0.96) was not significantly different from 1 ( $P > 0.6$ ); the  $y$ -intercept (0.18) was significantly different from 0 ( $P < 0.03$ ). In addition, the distribution of  $R_1/R_0$  predicted from the measured values of  $V_1/V_0$  and  $p$  was significantly bimodal (Hartigan's dip test,  $P < 0.05$ ; not shown). Analysis of the data using Mechler and Ringach's original model in which threshold was the free parameter, rather than the power-law exponent  $p$ , is shown in Supplementary Note online, and yields analogous results.

### The $V_1/V_0$ -to- $R_1/R_0$ transformation in single cells

Our analysis thus far rests on the shape of the relationship between  $V_1/V_0$  and  $R_1/R_0$  in a population of neurons when each cell is stimulated by its preferred orientation and spatial frequency. The power of the model in predicting the observed  $V_1/V_0$  is suggestive, but it does not eliminate the possibility that yet a third parameter, which covaries with  $V_1/V_0$  and  $p$  from cell to cell, could be a hidden source of varia-

could not be identified from their  $V_1/V_0$  values alone. Neither were the individual components,  $V_1$  and  $V_0$ , bimodally distributed (Fig. 3c,d). In addition, the  $V_1$  and  $V_0$  components were poorly correlated with one another both in the entire sample ( $r = 0.33$ ) and within the subsets of each cell type, as defined by the  $R_1/R_0$  histogram ( $r = 0.52$  in simple cells;  $r = 0.38$  in complex cells).

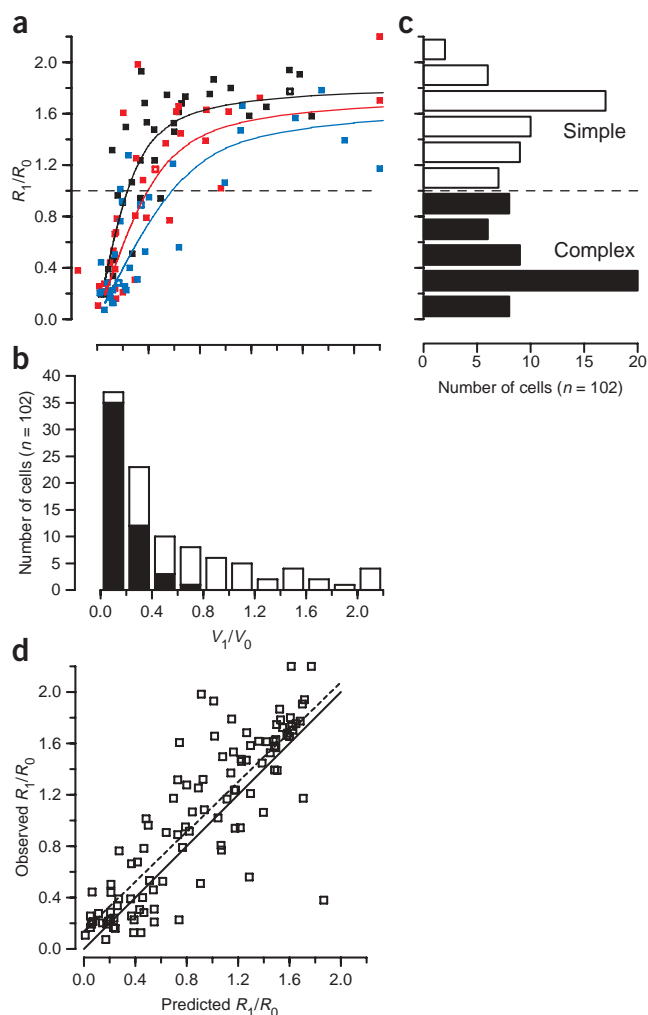
Next, we examined the spike thresholds of the two populations, with the thought that a dichotomy in threshold between simple and complex cells might account for the bimodal distribution of  $R_1/R_0$ .

**Figure 4** The nonlinear transformation from the voltage modulation ratio to the firing rate modulation ratio in primary visual cortex. (a) The voltage modulation ratio (abscissa) and firing rate modulation ratio (ordinate) are plotted for each cell in our sample population. Neurons were grouped by the exponent  $p$  that best fit the potential-to-firing rate relationship:  $p < 2.75$  (blue symbols),  $p > 3.5$  (black symbols) and  $p$  intermediate between these values (red symbols). The separation values were chosen to assure the same number of cells was found in each group. Blue, red and black lines indicate the predicted relationship between the potential modulation ratio and the rate modulation ratio for exponent values of 2, 3 and 5. Rate and potential modulation ratios greater than 2.2 are marked as 2.2. A single neuron had a negative voltage modulation ratio (due to a hyperpolarizing  $V_0$  response to the optimal grating). The example neurons from **Figure 2** are marked with open symbols. The distribution of the (b) voltage modulation ratio and (c) firing rate modulation ratio. Open and filled parts of bars indicate subsets of cells classified by the spike rate modulation as simple and complex cells. (d) Predicted and actual firing rate modulation ratios. The predicted firing rate modulation ratio is derived from the voltage modulation ratio and the exponent value. The solid line indicates a perfect relationship (identity) between the predicted and actual firing rate modulation ratios. The dashed line shows the linear regression between the predicted and actual firing rate modulation ratios.

tion in  $R_1/R_0$ . To test for this possibility, we stimulated each of a subset of cells with gratings of different spatial frequencies, which elicit responses of differing  $V_1/V_0$  and  $R_1/R_0$  values<sup>17–22</sup>. In complex cells, for example, low spatial frequency gratings often evoked responses that were modulated<sup>18</sup>. Although these responses were weaker than the responses evoked by the optimal spatial frequency, they were simple-like in that they were strongly modulated. The modulation occurs because the bars of the grating are comparable in width to the receptive field itself. Conversely, **Figure 5a–c** shows an example of a simple cell in which the spike modulation ratio decreases to complex-like levels at spatial frequencies much higher than the optimal. The cycle-averaged responses of spike rate and membrane potential are shown for this cell at seven different spatial frequencies in **Figure 5a**; spatial frequency tuning curves for  $V_1$  and  $V_0$  (membrane potential) and for  $R_1$  and  $R_0$  (spike rate) are shown in **Figure 5b** and **c**.

When  $R_1/R_0$  for the cell in **Figure 5a–c** is plotted against  $V_1/V_0$  for each spatial frequency (**Fig. 5d**), the data points cluster near the theoretical curve associated with the cells' measured power-law exponent  $p$  (3.1). Note that this theoretical curve is not a fit to the points in the graph, but is derived completely independently: the curve is based on the power-law fit to the measured relationship between membrane potential and firing rate, similar to those shown in **Figure 2d**. And yet, the theoretical curve conforms reasonably well to the observed relationship between  $V_1/V_0$  and  $R_1/R_0$ .

Similar results are shown in **Figure 5e–l** for eight other cells in which  $V_1/V_0$  varied with spatial frequency. For each cell, the preferred spatial frequency, and therefore the frequency at which the cell was classified as simple or complex, is shown by the open symbol. Over the nine illustrated cells, the values of  $R_1/R_0$  predicted from  $V_1/V_0$  and  $p$  (smooth curve) were closely correlated with measured  $R_1/R_0$ . Linear regression analysis of predicted versus measured values found  $R^2 = 0.71$ , slope = 0.91 (not significantly different from 1,  $P > 0.5$ ) and  $y$ -intercept = 0.13 (significantly different from 0,  $P < 0.05$ ). In several cells (**Fig. 5d, f, g** and **l**),  $V_1/V_0$  varied over a wide enough range to exhibit both the expansive and compressive portions of the relationship between  $V_1/V_0$  and  $R_1/R_0$ . In the remaining cells, the changes only covered the expansive or compressive regions of the theoretical curve. In almost all cases, the changes in  $R_1/R_0$  were large enough to carry the responses across the dividing line between simple-like and complex-like behavior (horizontal dotted line). That the model can



account for such a wide range of values of  $R_1/R_0$  in single cells supports the proposal that threshold alone gives rise to the transformation between  $V_1/V_0$  and  $R_1/R_0$ .

### Distinguishing simple and complex cells from spatial maps

The data presented thus far indicate that responses to drifting gratings, when measured intracellularly, do not form a bimodal distribution. Hubel and Wiesel, however, originally defined simple and complex neurons not by using drifting grating, but by using flashing dark and bright bars. Their primary criteria for identifying a simple cell were (i) that ON and OFF responses were segregated into separate subfields and (ii) that bright and dark stimuli antagonized one another<sup>1,2</sup>. In complex cells, ON and OFF responses overlapped. Although the modulation ratio in response to drifting gratings is thought to correspond closely to the degree of spatial segregation and antagonism of ON and OFF subfields, this correspondence has only been measured for the spike output<sup>6,19,21–23</sup>; it has not been assessed from the pattern of synaptic inputs.

We have therefore examined the membrane potential responses of 287 neurons to bright and dark spots flashed within the receptive field<sup>24–28</sup>. In 92 of these neurons, we also mapped the receptive fields from spiking responses. Receptive field maps are shown for four neurons in **Figure 6**. For each cell, four maps are shown, one each from membrane potential responses (with spikes removed) to bright and

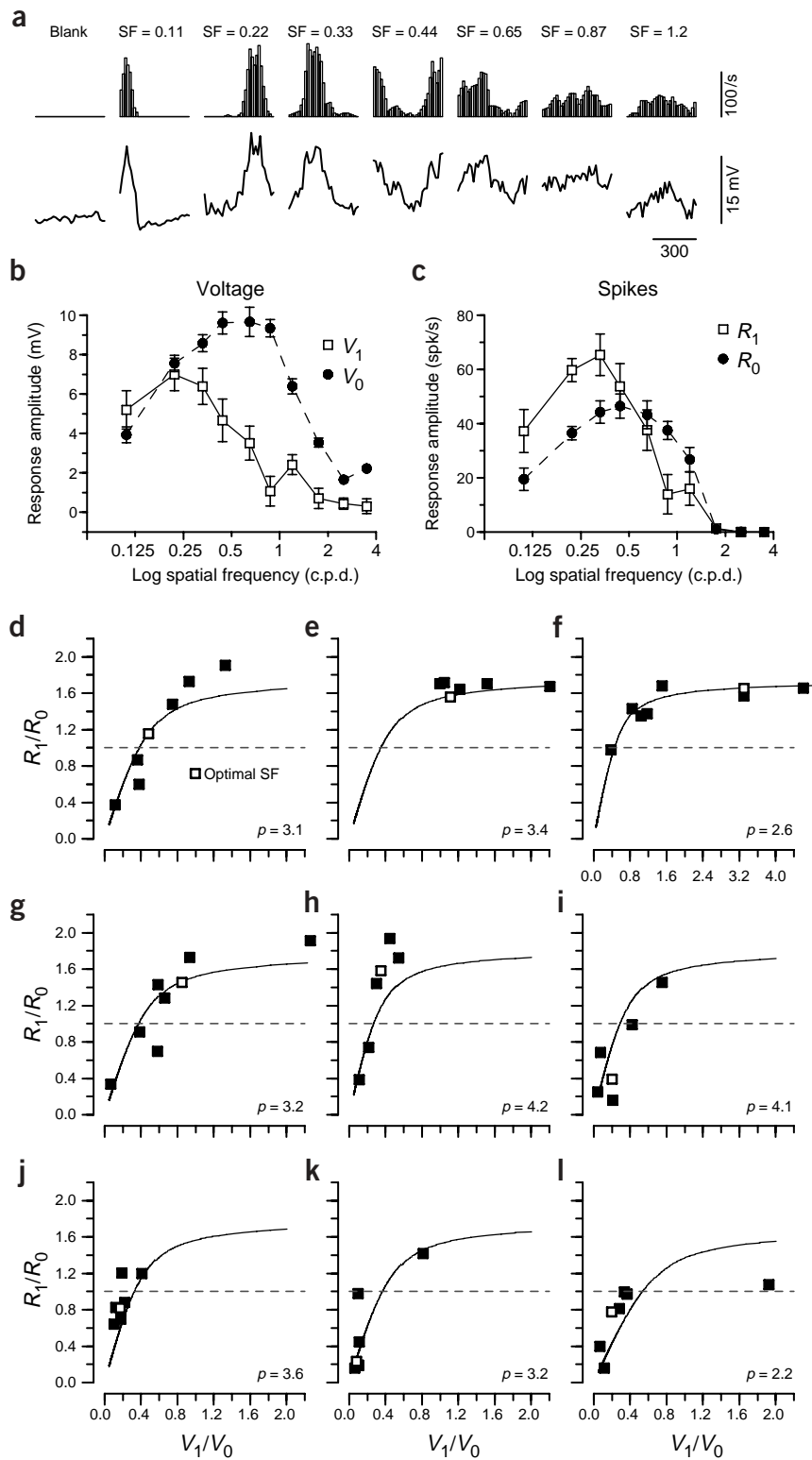


**Figure 5** The transformation between voltage modulation ratio and the firing rate modulation ratio in single cells. **(a)** Cycle averages of the firing rate response (top panels) and the membrane potential response to gratings of fixed (optimal) orientation, 2 Hz temporal modulation and different spatial frequencies (SF) for a single cell. **(b)** The  $V_1$  and  $V_0$  values shown as a function of the spatial frequency of the stimulus. **(c)** The corresponding  $R_1$  and  $R_0$  for the same cell. **(d)** For each spatial frequency that produced a measurable spike response, the voltage modulation ratio is plotted against the firing rate modulation ratio for the same cell shown in (a–c). The solid line indicates the model prediction given the exponent  $p$  that was estimated from the cell’s input-output function (not shown). The open symbol indicates the modulation ratios for the spatial frequency that elicited the largest  $R_0$ . **(e–l)** Same as shown in **(d)** for eight other neurons. The relationship between predicted and actual firing rate modulation ratios for the group of cells was high ( $R^2 = 0.71$ , slope = 0.91, not significantly different from 1 ( $P > 0.5$ ),  $y$ -intercept = 0.13, significantly different from 0 ( $P < 0.05$ )). The cells included both simple and complex cells as defined by  $R_1/R_0$  measured with the grating of optimal spatial frequency.

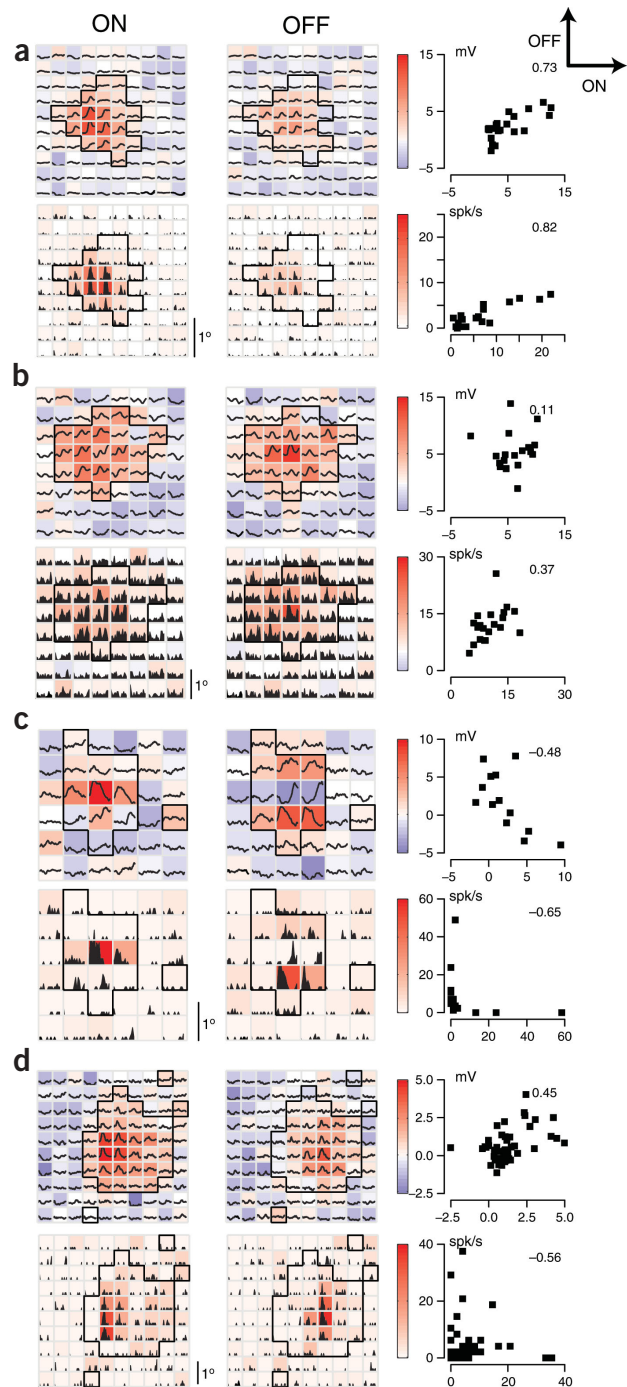
from potential and spike rate. The cell in **Figure 6c** is a classical simple cell with completely nonoverlapping ON and OFF subfields, again as defined both from potential and spike rate. The cell in **Figure 6b** is a complex cell as defined from its completely overlapping spiking ON and OFF responses, but the ON and OFF membrane potential responses are only partially overlapping. Finally, the cell in **Figure 6d** is a simple cell as defined by the nonoverlapping spiking ON and OFF responses, but has almost completely overlapping ON and OFF membrane potential responses. As shown previously<sup>29</sup>, the receptive fields derived from membrane potential responses were commonly larger than those derived from spike responses.

To quantify the overlap between ON and OFF regions, we first identified those spatial locations in which either a bright or dark stimulus elicited a significant membrane depolarization (outlined regions in the maps of **Fig. 6**; see Methods). We then plotted the amplitude of the ON response against the amplitude of the OFF response at each of these locations, both for membrane potential and for spike rate. The correlation coefficients derived from each

dark stimuli (upper right and left maps), and spiking rate responses to bright and dark stimuli (lower right and left maps). The background of each trace is color-coded for the amplitude of the responses. The four cells show the full range of spatial overlap found in our sample. The cell in **Figure 6a** is a classical complex cell with almost completely overlapping ON and OFF subfields as defined both

scatter plot are a strong indication of subregion overlap between ON and OFF response. For classical complex cells, ON responses are highly correlated with OFF responses, which results in a high correlation coefficient (between 0 and 1). The cell in **Figure 6a**, for example, has correlation coefficients much greater than zero for both membrane potential and spike rate. For classical simple cells, ON

**Figure 6** ON and OFF spatial maps for both membrane potential and spikes. **(a)** The membrane potential responses of a neuron evoked by bright (top left panel) or dark stimuli (middle left panel). The traces indicate the stimulus-averaged membrane potential for a 135-ms duration following the stimulus onset for each spatial location. The color at each spatial location indicates the membrane potential in the analysis period, averaged between 50 and 80 ms after the stimulus was flashed. The significance region (black outline) selected for further analysis consisted of spatial locations in which either a dark or bright stimulus elicited a significant depolarization relative to the resting potential of the neuron ( $t$ -test,  $P < 0.05$ ). The bottom two maps show spiking responses as stimulus-averaged spike rate histograms. The scattergrams to the right of the maps plot the amplitude of the ON response against the amplitude of the OFF response for each location within the significance region. Correlation coefficients for the scattergrams are shown at the upper right. **(b–d)** Different example neurons, same format. In response to moving gratings, the example neurons in panels **a** and **b** had  $R_1/R_0$  values less than 1 and so were considered complex, whereas those in **c** and **d** had  $R_1/R_0$  values greater than 1 and thus considered simple.



responses overlap little with OFF responses, which results in correlation coefficients between  $-1$  and  $0$ . The cell in **Figure 6c**, for example, has correlation coefficients less than zero for both membrane potential and spike rate.

All four parameters, modulation indices and spatial segregation for membrane potential and spike rate are compared in **Figure 7**. A histogram of the spatial correlation constructed from spiking responses is shown in **Figure 7a**. This distribution is significantly bimodal (Hartigan's dip test,  $P < 0.05$ ), as has been observed in extracellular recordings from monkey visual cortex<sup>2,30</sup>. The spatial correlation for membrane potential (**Fig. 7h**) was not bimodal (Hartigan's dip test,  $P > 0.2$ ), but instead had a largely flat distribution. The relationship between the spatial correlation for spike rate and spatial correlation for membrane potential is shown in **Figure 7f**. Together, **Figure 7a, f** and **h** show that the transformation between membrane potential and spike rate enhances the difference between simple and complex cells. There is a strong correlation between these two measures, but there are many fewer cells with spike-defined correlations between  $-0.2$  and  $0.2$  than there are cells with potential-defined correlations in this range. That is, most cells with intermediate potential-defined correlations (near zero) were either more simple (**Fig. 6d**) or more complex (**Fig. 6b**) in their spiking responses, relative to their membrane potential responses. For the cell in **Figure 6b**, for example, the correlation coefficient for potential is near zero because many of the locations with ON potential responses showed no potential response to OFF stimuli. Since many of the ON responses that lack corresponding OFF responses are subthreshold, however, they disappear in the spike map, and the ON and OFF spiking responses become more highly correlated. In **Figure 6d**, potential responses are highly correlated, but the largest ON and OFF responses are slightly offset spatially. Therefore, when threshold is applied, ON spike responses are absent from the right-hand portion of the receptive field, whereas OFF spike responses are absent from the left-hand portion of the receptive field. Thus, the cell becomes more simple in its spike responses than it is in its potential responses.

A comparison of the spatial correlation and the modulation ratio when both are based on spiking responses is shown in **Figure 7c**. As expected, there was a significant correlation between these two measures ( $R^2 = 0.51$ ). Eighty-eight percent of the cells that were classified as simple or complex by  $R_1/R_0$  were classified similarly by spiking spatial correlation. Thus, the  $R_1/R_0$  metric for cell classification to a large extent reflects the degree of subfield overlap measured

from spikes<sup>6,19</sup>. The same is not true for membrane potential. There is a poor correlation ( $R^2 = 0.25$ ) between  $V_1/V_0$  and spatial correlation based on membrane potential (**Fig. 7g**), and neither measure is bimodal.

Note that our measure of correlation between ON and OFF spike responses is performed on spatial locations that elicited significant ON or OFF membrane potential responses (outlines in the maps of **Fig. 6**), whether or not significant spiking responses were obtained from these same locations. We have also used a different method in which the spatial correlation coefficient for spiking was calculated from locations in which there were significant spiking responses (of

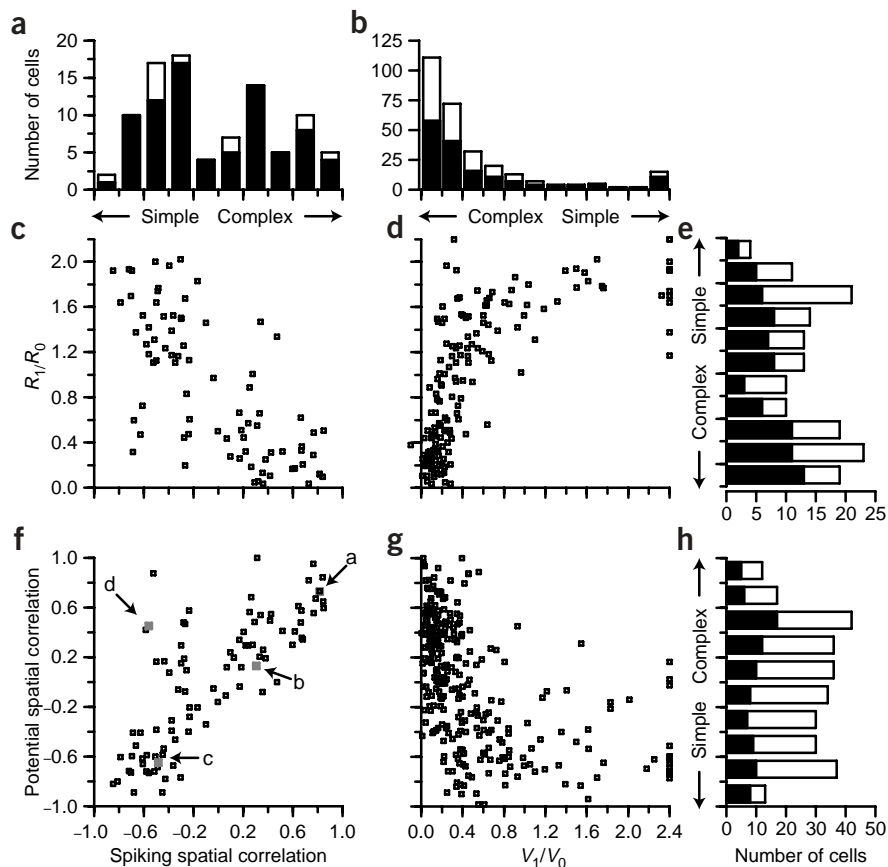


**Figure 7** A comparison of the various measures of grating modulation and spatial segregation of ON and OFF responses. **(a)** The distribution of the spatial correlation coefficient from spike rate responses. Filled bars indicate the neurons for which both  $R_1/R_0$  and the spatial correlation analysis was performed. The distribution is significantly bimodal (Hartigan's dip test,  $P < 0.05$ ). **(b)** The distribution of  $V_1/V_0$ . Filled bars indicate those neurons for which the spatial correlation of potential responses was analyzed. The distribution is not significantly bimodal (Hartigan's dip test,  $P > 0.5$ ). **(c)** The relationship between  $R_1/R_0$  and the spatial correlation coefficient from spike rate responses ( $n = 80$ ). **(d)** The relationship between  $R_1/R_0$  and  $V_1/V_0$  ( $n = 157$ ). **(e)** The distribution of  $R_1/R_0$ . The distribution is significantly bimodal (Hartigan's dip test,  $P < 0.05$ ). **(f)** The relationship between the spatial correlation coefficients from spike rate and membrane potential responses ( $n = 92$ ). Filled gray symbols and arrows correspond to the example neurons in **Figure 6**. **(g)** The relationship between  $V_1/V_0$  and the spatial correlation coefficients from membrane potential responses ( $n = 287$ ). **(h)** The distribution of the spatial correlation coefficients from membrane potential responses. The distribution is not significantly bimodal (Hartigan's dip test,  $P > 0.2$ ). Filled bars indicate those neurons for which spatial maps were obtained from spike responses.

either polarity). A bimodal distribution of spatial correlation based on spikes was found using either method.

## DISCUSSION

Our intracellular recordings indicate that the nonlinearity of the spike mechanism contributes directly to creating the dichotomy between simple and complex cells. The clear distinction between these two classes evident in the bimodal distribution of the spiking modulation index ( $R_1/R_0$ ) does not arise directly from a bimodal distribution in the membrane potential modulation index ( $V_1/V_0$ ). The bimodality in the spiking responses seems to arise from the nonlinear relationship between membrane potential and spike rate. This is not to say that there is no underlying difference in connectivity that gives rise to stronger or weaker degrees of modulation in the membrane potential responses; we found that 90% of simple cells (as defined by their spike output) had  $V_1$  components greater than 2 mV, whereas 78% of complex cells had  $V_1$  components of less than 2 mV (**Fig. 3d**). But both the  $V_1$  component by itself and the  $V_1/V_0$  ratio are unimodally distributed and so by themselves give no hint of there being two fundamentally distinct populations of cortical neurons. The appearance of bimodality in  $R_1/R_0$  depends on the match between the highly skewed distribution of  $V_1/V_0$  and the nonlinear transformation by the spike threshold. The threshold nonlinearity is therefore required to make simple and complex cells into distinct classes, identifiable from the distribution of a single parameter,  $R_1/R_0$ .

In constructing the theoretical relationship between  $V_1/V_0$  and  $R_1/R_0$ , we chose to model the transformation between membrane potential and spike rate as a power law. We differ in this regard from Mechler and Ringach, who used the more standard threshold-linear model of spiking. Most neurons, including neurons of primary visual

cortex, do behave in a threshold-linear fashion under controlled conditions such as the repeated injection of current pulses<sup>31</sup>. The large trial-to-trial variability in the responses of neurons of primary visual cortex, however, tends to smooth the average relationship between mean membrane potential and mean firing rate so that it approximates a power law<sup>14,15,32,33</sup>. Additional smoothing might originate from variations in threshold related to  $dV/dt$ <sup>34,35</sup>. Our results are not dependent on the use of the power law, however. As shown in the **Supplementary Note**, a threshold-linear function captures the  $V_1/V_0$ -to- $R_1/R_0$  relationship equally well, and indeed any similar expansive nonlinearity will likely do so. We attach no theoretical significance to the power law, but only use it as a convenient method to capture the numerical relationship between membrane potential and spike rate for the purposes of the model.

Measures of the modulation in the responses to gratings do not directly test whether classes of primary visual cortex neurons exist with distinct spatial organization of receptive fields. In Hubel and Wiesel's original classification scheme<sup>1</sup>, simple cells have spatially segregated ON and OFF subregions, while complex cells have overlapping ON and OFF subregions. Extracellular studies designed to quantify the spatial (or spatiotemporal) overlap of ON and OFF subregions of the receptive field using various stimuli have reported a bimodal distribution of a corresponding index quantity<sup>23,24,30,36</sup> (but see ref. 37). We have confirmed this finding in our measure of the spatial correlation between ON and OFF spiking responses. As with grating responses, however, the distinction between simple and complex cells was restricted to spiking responses; the distribution of the spatial correlation coefficient computed from membrane potential was not bimodal. Threshold, once again, seems to enhance the distinction between these two classes of cells. Although we have a qualitative

understanding of why this distinction occurs, as described for the cells in **Figure 6b** and **d**, we have yet to develop as detailed a model as Mechler and Ringach have done for grating responses.

The emergence of the simple/complex distinction from the effects of threshold is reminiscent of the threshold-based sharpening of selectivity for orientation, size and direction<sup>29,38,39</sup>, in essence, an ‘iceberg’ effect (albeit a complicated one) applied to a measure of spatial linearity. Unlike direction selectivity or orientation selectivity, however, threshold is creating a qualitative distinction between two classes of cells, rather than simply transforming one unimodal distribution into another. Our study is consistent with Hubel and Wiesel in that when one examines the spiking responses, there are two distinct classes of neurons, simple and complex, whether defined from the spatial segregation of ON and OFF responses or from the modulation of grating responses. Thus, simple and complex cells, at least for specific stimuli, are completely distinct from the point of view of their downstream target neurons. And yet our results suggest that these two classes emerge from a continuous distribution of synaptic inputs. That is, the continuous distribution of the character of membrane potential responses, as defined either from grating response or map segregation, reflects a continuum in the patterns of cortical connectivity, consistent with models of primary visual cortex built from circuits with variable strength of phase-insensitive cortical connectivity<sup>12,40</sup>.

These findings are not inconsistent with the hierarchical organization of cortex articulated by Hubel and Wiesel. Indeed, simple cells distinguished on the basis of spiking response are more likely to be found in the input layers of the cortex, layer 4 in particular<sup>3,4,41</sup>. Layer 4, in turn, projects heavily to the supragranular layers<sup>9,42</sup>, which contain a high proportion of complex cells. Nevertheless, the intracellular characterization of cortical neurons suggests that the distinction between the synaptic organization of simple and complex cells is one of degree rather than kind.

## METHODS

Recordings were obtained from area 17 in barbiturate-anesthetized, paralyzed young adult female cats (between 6 months and 1 year). All methods regarding the animal preparation received prior approval by Northwestern University’s Committee on Experimental Animal Research. Details of the preparation may be found elsewhere<sup>43</sup>.

Current clamp recordings were made with either sharp electrodes or patch electrodes in whole-cell configuration using an Axoclamp 2A amplifier (Axon Instruments). Electrodes were made using a Flaming/Brown micropipette puller (Sutter Instruments model p87) from borosilicate glass. Patch electrodes (6–13 M $\Omega$ ) were filled with 130 mM potassium gluconate, 2 mM MgCl<sub>2</sub>, 5 mM HEPES, 1.1 mM EGTA, 0.1 mM CaCl<sub>2</sub> and 3 mM magnesium ATP. Sharp electrodes were filled with 2 M potassium acetate.

Experiments were controlled using custom software (LabVIEW, National Instruments). The LabVIEW program controlled the digitization of the voltage and sent instructions to a Macintosh computer controlling the visual stimulus. Stimuli were generated on a Viewsonic video monitor (100 Hz refresh rate; 20 cd/m<sup>2</sup> mean luminance) by the Macintosh computer running the Psychophysics toolbox libraries for Matlab (Mathworks)<sup>44,45</sup>.

Using drifting gratings, each neuron’s receptive field was initially characterized by its tuning for location, size, orientation and spatial frequency. The preferred stimulus was defined as the stimulus condition that evoked the largest average firing rate. Stimuli (2-s or 4-s presentations of each grating with 250-ms blanks preceding and following) were interleaved in pseudorandom order. Offline, firing-rate histograms were generated after detecting the spikes using a thresholded version of the membrane potential. Average potential responses were computed after spikes were removed from the potential signals using a 4-ms median filter<sup>39</sup>. The relationship between membrane and firing rate was fit using the power function  $R(V_m) = k[V_m - V_{rest}]_+^p$ , where  $V_m$

is the membrane potential,  $V_{rest}$  is the resting membrane potential (taken from the response to a blank stimulus),  $k$  is the gain factor and  $p$  is the exponent. The subscript “+” indicates rectification, i.e., that values below zero are set to zero. Trial averages of the membrane potential and firing rate were binned into 30-ms epochs before fitting the power function. In 97% of the neurons in our sample population (99/102), 95% confidence intervals for the exponent  $p$  did not overlap a value of 1.

After determining the spatial extent of the receptive field using gratings, we measured the receptive fields quantitatively using a sparse noise stimulus. An area of the screen, usually about 5° × 5°, which covered the receptive field, was divided into a grid of small squares. The luminance of one pixel at a time was then set to either twice the background luminance of the screen (ON stimulus) or 0 luminance (OFF stimulus) for 30–60 ms, with an interstimulus interval of a single frame refresh. Membrane potential traces and spiking responses were computed for each spatial location and polarity, by aligning the potential or spiking responses to the onset of the presentation of the spot and averaging the response that followed. Maps were derived from the average response to between 10 and 70 sequences of the sparse noise stimulus. The response amplitude was computed by averaging the response 50–80 ms after each spot was presented. Locations that elicited significant responses were identified by comparing the average response after a spot was presented to the response to a blank stimulus and testing for significance ( $t$ -test,  $P < 0.05$ ). The spatial correlation coefficient was computed using Pearson’s correlation coefficient<sup>46</sup>.

*Note: Supplementary information is available on the Nature Neuroscience website.*

## ACKNOWLEDGMENTS

We thank D.L. Ringach, J.D. Victor and K.D. Miller for comments on the manuscript. I. Lampl, D.C. Gillespie and J.S. Anderson participated in data collection. This work was supported by grants from the National Institutes of Health, the National Science Foundation and the Human Frontier Science Program.

## COMPETING INTERESTS STATEMENT

The authors declare that they have no competing financial interests.

Received 4 May; accepted 23 July 2004

Published online at <http://www.nature.com/natureneuroscience/>

- Hubel, D.H. & Wiesel, T.N. Receptive fields, binocular interaction and functional architecture in the cat’s visual cortex. *J. Physiol. (Lond.)* **160**, 106–154 (1962).
- Hubel, D.H. & Wiesel, T.N. Receptive fields and functional architecture of monkey striate cortex. *J. Physiol. (Lond.)* **195**, 215–243 (1968).
- Gilbert, C.D. Laminar differences in receptive field properties of cells in cat primary visual cortex. *J. Physiol. (Lond.)* **268**, 391–421 (1977).
- Ferster, D. & Lindstrom, S. An intracellular analysis of geniculo-cortical connectivity in area 17 of the cat. *J. Physiol. (Lond.)* **342**, 181–215 (1983).
- Hirsch, J.A. *et al.* Synaptic physiology of the flow of information in the cat’s visual cortex *in vivo*. *J. Physiol. (Lond.)* **540**, 335–350 (2002).
- Skottun, B.C. *et al.* Classifying simple and complex cells on the basis of response modulation. *Vision Res.* **31**, 1079–1086 (1991).
- De Valois, R.L., Albrecht, D.G. & Thorell, L.G. Spatial frequency selectivity of cells in macaque visual cortex. *Vision Res.* **22**, 545–559 (1982).
- Alonso, J.M., Usrey, W.M. & Reid, R.C. Rules of connectivity between geniculate cells and simple cells in cat primary visual cortex. *J. Neurosci.* **21**, 4002–4015 (2001).
- Alonso, J.M. & Martinez, L.M. Functional connectivity between simple cells and complex cells in cat striate cortex. *Nat. Neurosci.* **1**, 395–403 (1998).
- Martinez, L.M. & Alonso, J.M. Construction of complex receptive fields in cat primary visual cortex. *Neuron* **32**, 515–525 (2001).
- Spitzer, H. & Hochstein, S. Complex-cell receptive field models. *Prog. Neurobiol.* **31**, 285–309 (1988).
- Chance, F.S., Nelson, S.B. & Abbott, L.F. Complex cells as cortically amplified simple cells. *Nat. Neurosci.* **2**, 277–282 (1999).
- Mechler, F. & Ringach, D.L. On the classification of simple and complex cells. *Vision Res.* **42**, 1017–1033 (2002).
- Hansel, D. & van Vreeswijk, C. How noise contributes to contrast invariance of orientation tuning in cat visual cortex. *J. Neurosci.* **22**, 5118–5128 (2002).
- Miller, K.D. & Troyer, T.W. Neural noise can explain expansive, power-law nonlinearities in neural response functions. *J. Neurophysiol.* **87**, 653–659 (2002).
- Hartigan, J.A. & Hartigan, P.M. The dip test of unimodality. *Ann. Stat.* **13**, 70–84 (1985).
- De Valois, R.L. & De Valois, K.K. Spatial vision. *Annu. Rev. Psychol.* **31**, 309–341 (1980).
- Movshon, J.A., Thompson, I.D. & Tolhurst, D.J. Receptive field organization of complex cells in the cat’s striate cortex. *J. Physiol. (Lond.)* **283**, 79–99 (1978).

19. Dean, A.F. & Tolhurst, D.J. On the distinctness of simple and complex cells in the visual cortex of the cat. *J. Physiol. (Lond.)* **344**, 305–325 (1983).
20. Foster, K.H., Gaska, J.P., Nagler, M. & Pollen, D.A. Spatial and temporal frequency selectivity of neurones in visual cortical areas V1 and V2 of the macaque monkey. *J. Physiol. (Lond.)* **365**, 331–363 (1985).
21. Glezer, V.D., Tsherbach, T.A., Gauselman, V.E. & Bondarko, V.M. Linear and non-linear properties of simple and complex receptive fields in area 17 of the cat visual cortex. A model of the field. *Biol. Cybern.* **37**, 195–208 (1980).
22. Glezer, V.D., Tsherbach, T.A., Gauselman, V.E. & Bondarko, V.M. Spatio-temporal organization of receptive fields of the cat striate cortex. The receptive fields as the grating filters. *Biol. Cybern.* **43**, 35–49 (1982).
23. Kagan, I., Gur, M. & Snodderly, D.M. Spatial organization of receptive fields of V1 neurons of alert monkeys: comparison with responses to gratings. *J. Neurophysiol.* **88**, 2557–2574 (2002).
24. Conway, B.R. & Livingstone, M.S. Space-time maps and two-bar interactions of different classes of direction-selective cells in macaque V-1. *J. Neurophysiol.* **89**, 2726–2742 (2003).
25. Reid, R.C., Soodak, R.E. & Shapley, R.M. Directional selectivity and spatiotemporal structure of receptive fields of simple cells in cat striate cortex. *J. Neurophysiol.* **66**, 505–529 (1991).
26. Volgushev, M., Vidyasagar, T.R. & Pei, X. A linear model fails to predict orientation selectivity of cells in the cat visual cortex. *J. Physiol. (Lond.)* **496**, 597–606 (1996).
27. Lampl, I., Anderson, J.S., Gillespie, D.C. & Ferster, D. Prediction of orientation selectivity from receptive field architecture in simple cells of cat visual cortex. *Neuron* **30**, 263–274 (2001).
28. Jones, J. & Palmer, L. The two-dimensional structure of simple receptive fields in cat striate cortex. *J. Neurophysiol.* **58**, 1187–1211 (1987).
29. Bringuier, V., Chavane, F., Glaeser, L. & Fregnac, Y. Horizontal propagation of visual activity in the synaptic integration field of area 17 neurons. *Science* **283**, 695–699 (1999).
30. Schiller, P.H., Finlay, B.L. & Volman, S.F. Quantitative studies of single-cell properties in monkey striate cortex. I. Spatiotemporal organization of receptive fields. *J. Neurophysiol.* **39**, 1288–1319 (1976).
31. Carandini, M., Mechler, F., Leonard, C.S. & Movshon, J.A. Spike train encoding by regular-spiking cells of the visual cortex. *J. Neurophysiol.* **76**, 3425–3441 (1996).
32. Heeger, D.J. Half-squaring in responses of cat striate cells. *Vis. Neurosci.* **9**, 427–443 (1992).
33. Anderson, J.S., Lampl, I., Gillespie, D.C. & Ferster, D. The contribution of noise to contrast invariance of orientation tuning in cat visual cortex. *Science* **290**, 1968–1972 (2000).
34. Hodgkin, A.L. & Huxley, A.F. A quantitative description of membrane current and its application to conduction and excitation in nerve. *J. Physiol. (Lond.)* **117**, 500–544 (1952).
35. Azouz, R. & Gray, C.M. Dynamic spike threshold reveals a mechanism for synaptic coincidence detection in cortical neurons *in vivo*. *Proc. Natl. Acad. Sci. USA* **97**, 8110–8115 (2000).
36. Heggelund, P. Quantitative studies of the discharge fields of single cells in cat striate cortex. *J. Physiol. (Lond.)* **373**, 277–292 (1986).
37. Mata, M.L. & Ringach, D.L. Spatial overlap of 'on' and 'off' subregions and its relation to response modulation ratio in macaque primary visual cortex. *J. Neurophysiol.* (in the press).
38. Carandini, M. & Ferster, D. Membrane potential and firing rate in cat primary visual cortex. *J. Neurosci.* **20**, 470–484 (2000).
39. Jagadeesh, B., Wheat, H.S., Kontsevich, L.L., Tyler, C.W. & Ferster, D. Direction selectivity of synaptic potentials in simple cells of the cat visual cortex. *J. Neurophysiol.* **78**, 2772–2789 (1997).
40. Tao, L., Shelley, M., McLaughlin, D. & Shapley, R. An egalitarian network model for the emergence of simple and complex cells in visual cortex. *Proc. Natl. Acad. Sci. USA* **101**, 366–371 (2004).
41. Hirsch, J.A., Alonso, J.M., Reid, R.C. & Martinez, L.M. Synaptic integration in striate cortical simple cells. *J. Neurosci.* **18**, 9517–9528 (1998).
42. Gilbert, C.D. Microcircuitry of the visual cortex. *Annu. Rev. Neurosci.* **6**, 217–247 (1983).
43. Chung, S. & Ferster, D. Strength and orientation tuning of the thalamic input to simple cells revealed by electrically evoked cortical suppression. *Neuron* **20**, 1177–1189 (1998).
44. Brainard, D.H. The Psychophysics Toolbox. *Spat. Vis.* **10**, 433–436 (1997).
45. Pelli, D.G. The VideoToolbox software for visual psychophysics: transforming numbers into movies. *Spat. Vis.* **10**, 437–442 (1997).
46. Sokal, R.R. & Rohlf, F.J. *Biometry: The Principles and Practice of Statistics in Biological Research* (W.H. Freeman, New York, 1995).